

Letter

Error Decomposition of Remote Sensing Soil Moisture Products Based on the Triple-Collocation Method Introducing an Unbiased Reference Dataset: A Case Study on the Tibetan Plateau

Jian Kang ¹, Rui Jin ^{1,2,*}, Xin Li ^{2,3}  and Yang Zhang ¹

¹ Key Laboratory of Remote Sensing of Gansu Province, Heihe Remote Sensing Experimental Research Station, Northwest Institute of Eco-Environment and Resources, Chinese Academy of Sciences, Lanzhou 730000, China; kangjian@nieer.ac.cn (J.K.); zhangyang@lzb.ac.cn (Y.Z.)

² CAS Center for Excellence in Tibetan Plateau Earth Sciences, Beijing 100101, China; lixin@lzb.ac.cn

³ Institute of Tibetan Plateau Research, Chinese Academy of Sciences, Beijing 100101, China

* Correspondence: jinrui@lzb.ac.cn; Tel.: +86-931-496-7724

Received: 13 July 2020; Accepted: 19 September 2020; Published: 21 September 2020



Abstract: Remote sensing (RS) soil moisture (SM) products have been widely used in various environmental studies. Understanding the error structure of data is necessary to properly apply RS SM products in trend and variation analysis and data fusion. However, a spatially continuous assessment of RS SM datasets is impeded by the limited spatial distribution of ground-based observations. As an alternative, the RS apparent thermal inertia (ATI) data related to the SM are transformed into SM values to expand the validation space. To obtain error components, the ATI-based SM along with the Soil Moisture Active Passive Mission (SMAP) and Advanced Microwave Scanning Radiometer 2 (AMSR2) SM are applied with the triple-collocation (TC) method to evaluate the RS SM data regarding random errors and amplitude variances at the regional scale. When the ATI-based SM is regarded as the reference data, the amplitude biases of the other two datasets are determined. The mean bias is also estimated by calculating the mean value difference between the ATI-based and validated RS SM. The results show that the ATI-based SM is a reliable source of reference data that, when combined with the TC method, can correctly estimate the error structure of RS SM datasets in wide space, promoting the reasonable application and calibration of RS SM datasets.

Keywords: error decomposition; random error; remote sensing product; systematic error; soil moisture; triple-collocation

1. Introduction

Soil moisture (SM) plays an important role in the climate system and influences water, energy, and carbon cycles [1–3]. Long-term and large-scale SM monitoring can promote research on SM-climate interactions [4]. With the growth of research interest on the relationship between SM and climate in recent years, the demand for SM observations has increased [5]. Satellite remote sensing (RS) technology has been considered a principal way to provide long time series of SM datasets with 25–40 km of spatial resolution at the global scale [6]. In recent decades, numerous satellite sensors have enriched current SM datasets in real time. Due to several factors, e.g., platform design, instrument configuration, and retrieval algorithm, different RS SM datasets have their own characteristics [7], which are expressed in their systematic and random errors, and the systematic error consists of mean bias (first-order) and amplitude bias (second-order). Therefore, understanding the error structure of RS SM datasets is beneficial for mining valuable information, e.g., in data fusion studies [8,9].

RS SM products can generally be evaluated by referencing ground-based observations, model-based SM data, and other RS SM products [10]. The validation results vary with the reference data because of the different SM representations [11]. In-situ measurements are always regarded as true values with which to evaluate RS products. Although ground-based observations are the ideal choice, the distribution of ground sites is limited to a small spatial extent, meaning that error structure analysis cannot be performed in a wide space. Due to high spatiotemporal continuity, modeled and RS SM products have been widely used as alternative reference data [12–17]. However, the scale dependence of input parameters in the simulation and retrieval SM leads to difficulty in quantifying the uncertainties of modeled and RS SM products [18,19], which is caused by the imprecise expression of subgrid heterogeneity information. To capture the spatial heterogeneity of SM within a large-scale grid, RS ancillary data related to SM with a high spatial resolution relative to RS SM products, e.g., terrain data [20] and optical RS data [21–25], are employed; therefore, they have the potential to estimate a reliable reference dataset for decomposing the errors of RS SM products.

If the reference data are determined, the bias of the temporal mean is easily estimable, and the cumulative distribution function (CDF) based on piecewise linear matching has been applied in calibrating the anomaly (the remainder when removing the mean value from the temporal data) [11,26]; however, this adjustment is not truly a calibration of the amplitude because the anomaly includes the random error [27]. Therefore, the key to evaluating the amplitude is to isolate the random error from the anomaly. Recently, the triple-collocation (TC) method has become popular in the evaluation of RS SM products [28–30], as this method can simultaneously estimate the random errors of multiple collocated datasets. Furthermore, the amplitude bias between RS SM products and the reference data can also be estimated by the TC method, which avoids the influences of random errors. Thus, it is feasible to obtain error components using the TC method, the key to which is to obtain reference data.

In this paper, the RS ancillary data related to the SM are transformed into SM values by establishing the relationship with in-situ measurements, which expands the ground-based observation information across a wide spatial extent. Transformed SM data are introduced into the TC method as reference data to decompose the errors of RS SM products for estimating the systematic and random error components. This study focuses on providing a feasible scheme for obtaining the error structure of RS SM products.

2. Materials and Methods

2.1. Study Area and Data

The study area is situated on the Tibetan Plateau (TP), which has an average elevation of approximately 4000 m. The temperature increases from west to east, and precipitation shows a decreasing trend from southeast to northwest. According to the International Geosphere-Biosphere Programme (IGBP) classification scheme, the TP is mainly covered by grasslands and bare (less than 10% vegetation), accounting for more than 90% of the total area.

There are a number of observation sites on the TP, which is beneficial to the study on the error decomposition of remotely sensed SM products. As shown in Figure 1, the SM observation networks are deployed in Ngari, Naqu, Maqu, and Babao [22,31]. The differences in the temporal variation among four observation networks are shown in Figure 2. The in-situ measurements obtained at a depth of 5 cm from May 2015 to September 2015 are adopted. The Moderate Resolution Imaging Spectroradiometer (MODIS) albedo (MCD43B3) and land surface temperature (LST; MOD11A1 and MYD11A1) data are used to calculate the apparent thermal inertia (ATI) with a spatial resolution of 1 km, which is transformed into SM values by building the relationship with SM measurements from Ngari and Maqu networks separately covering bare areas and grasslands. The ATI-based SM is considered the reference data, and its applicability on the TP is validated using the relative SM truth estimated using the Voronoi diagram method and the modeled surface SM with $0.25^\circ \times 0.25$ spatial resolution from the Global Land Data Assimilation System (GLDAS) [32] of the National Aeronautics

and Space Administration (NASA) in the Naqu and Babao regions. Two microwave RS SM products derived from the Advanced Microwave Scanning Radiometer 2 (AMSR2) [33] and Soil Moisture Active Passive Mission (SMAP) [34] as experimental datasets combined with the ATI-based SM are adopted to perform error decomposition based on the TC method.

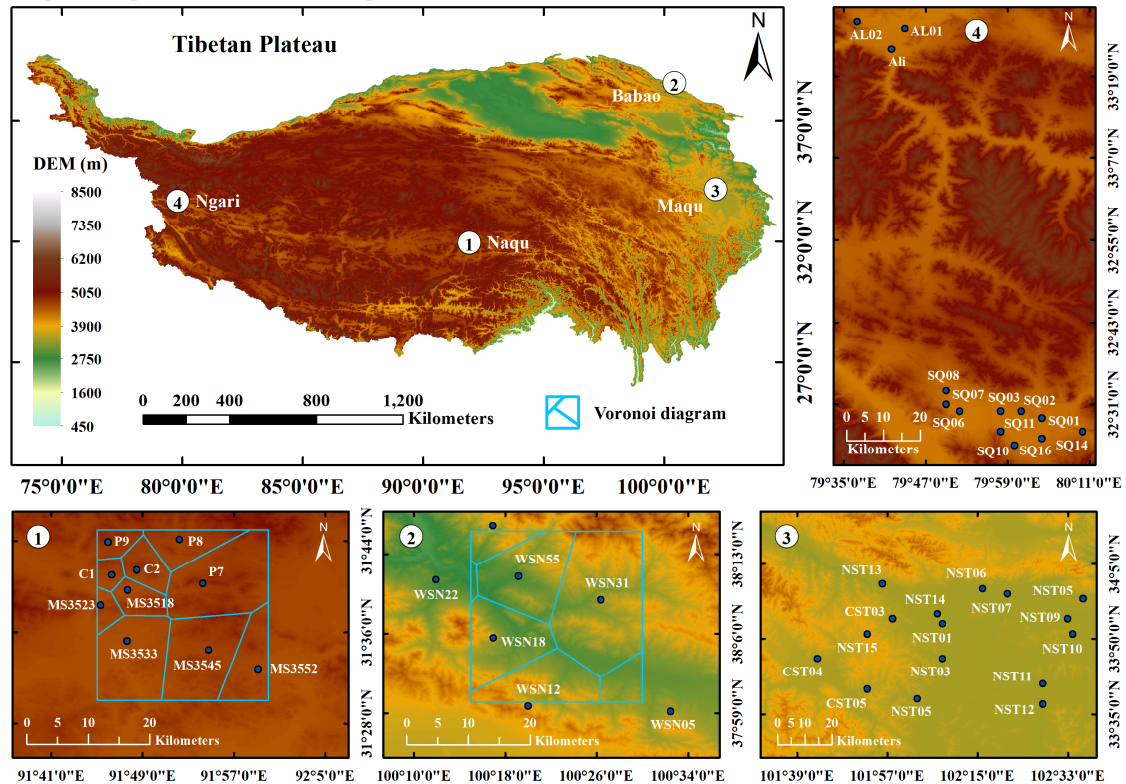


Figure 1. Map of the study area and the spatial distributions of soil moisture (SM) observation sites.

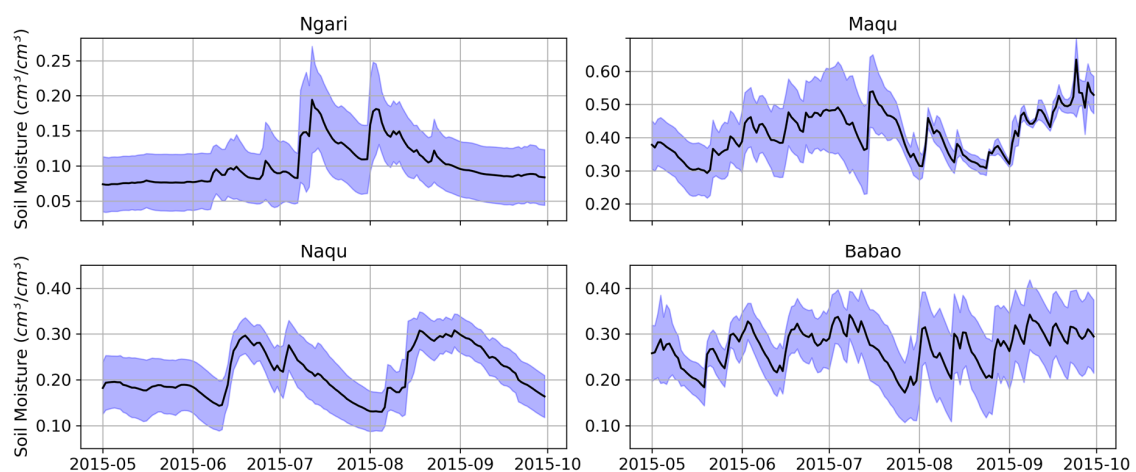


Figure 2. Temporal changes in the mean and standard deviation in four observation networks.

2.2. Methodology

2.2.1. Error Decomposition

Validation of RS SM products is generally based on temporal information. The error structure of temporal data can be characterized by systematic and random errors, and the systematic error

has usually been represented as the biases of the temporal mean and amplitude range in previous validation cases. Therefore, the time series of RS SM data S_i can consist of three components:

$$S_i = \beta_i + \alpha_i\theta + \varepsilon_i \quad (1)$$

where β_i is the temporal mean value, α_i is the multiplicative factor of the true amplitude process θ with $E(\theta) = 0$, and ε_i is the additive zero-mean random noise.

The error of S_i can be partitioned via the root-mean-square error (RMSE) between S_i and the reference data:

$$\text{RMSE}(S_i, S_j) = \sqrt{(\beta_i - \beta_j)^2 + (\alpha_i - \alpha_j)^2 \text{var}(\theta) + \text{var}(\varepsilon_i) + \text{var}(\varepsilon_j)} \quad (2)$$

where $\text{var}(\cdot)$ computes the temporal variance. The last two items are the variances of the random errors. It is assumed that the random errors are not cross correlated with each other in Equation (2) or with the other terms in Equation (1). If S_j is the reference data, error metrics of each component of S_i can be expressed as follows [35]:

$$\left\{ \begin{array}{l} \beta_{ij} = \beta_i - \beta_j \\ \alpha_{ij} = \alpha_i / \alpha_j \\ \sigma_{\varepsilon_i} = \sqrt{\text{var}(\varepsilon_i)} \\ \text{RMSE}(\alpha_i\theta, \alpha_j\theta) = (\alpha_i - \alpha_j)^2 \text{var}(\theta) \end{array} \right. \quad (3)$$

where β_{ij} is the temporal mean bias of S_j and α_{ij} is the amplitude bias of S_i with $\alpha_j = 1$. The random error of S_i is measured using the standard deviation of random error σ_{ε_i} . The uncertainty of amplitude $\alpha_i\theta$ is expressed as the RMSE between $\alpha_i\theta$ and $\alpha_j\theta$.

In this paper, the error structures of AMSR2 and SMAP are analyzed using the TC method to estimate the parameters $\text{var}(\varepsilon_i)$, $\text{var}(\alpha_i\theta)$, and α in combination with a reference dataset [36]:

$$\begin{bmatrix} \sigma_{\varepsilon_1} \\ \sigma_{\varepsilon_2} \\ \sigma_{\varepsilon_3} \end{bmatrix} = \begin{bmatrix} \sqrt{C_{11} - C_{12}C_{13}/C_{23}} \\ \sqrt{C_{22} - C_{12}C_{23}/C_{13}} \\ \sqrt{C_{33} - C_{13}C_{23}/C_{12}} \end{bmatrix} \quad (4)$$

where $\sigma_{\varepsilon_i}^2$ is the same as $\text{var}(\varepsilon)$ in Equation (2) and C_{ij} computes the covariance between S_i and S_j . The product term of C_{ij} represents the variances of the amplitudes $\alpha_i\theta$:

$$\begin{bmatrix} \text{var}(\alpha_1\theta) \\ \text{var}(\alpha_2\theta) \\ \text{var}(\alpha_3\theta) \end{bmatrix} = \begin{bmatrix} C_{12}C_{13}/C_{23} \\ C_{12}C_{23}/C_{13} \\ C_{13}C_{23}/C_{12} \end{bmatrix} \quad (5)$$

When S_1 is treated as the reference data, the multiplicative factors of the other two temporal datasets are estimated as follows:

$$\alpha_2 = \frac{C_{23}}{C_{13}}, \alpha_3 = \frac{C_{23}}{C_{12}} \quad (6)$$

The multiplicative factors of S_2 and S_3 representing the amplitude biases can be solved without being affected by random errors.

2.2.2. Determination of the Reference Dataset

The key to error decomposition based on the TC method is to select a reliable reference dataset. In-situ measurements have always been considered as reference data but have a limited spatial extent. To obtain the error structure of RS SM products in wide space, the extra ancillary data need be introduced. Optical satellite sensors with thermal infrared channels have received a great deal of attention for representing regional SM at the fine spatial scale. In this paper, the remotely sensed ATI

related to the surface water status is considered ancillary data to capture the spatial heterogeneity of SM and is computed with the MODIS albedo and LST products as follows [37]:

$$\tau = A \frac{1 - \omega}{\Delta T} \quad (7)$$

where A is the solar correction factor, ω is the surface albedo derived from the MODIS albedo product, and ΔT is the maximum daily amplitude of the LST calculated with the MODIS LST product. To extend the in-situ measurement information to a wider space, an empirical relationship between the in-situ SM measurements $\theta_{in-situ}$ and the ATI τ can be formulated as follows:

$$\theta_{in-situ} = f(\tau) + \eta \quad (8)$$

where η represents the modeling residuals. The relationship function $f(\cdot)$ is used to transform the ATI to SM. The ATI-based SM is resampled by averaging the SM obtained from Equation (8) within pixels of 0.25° .

3. A Case Study on the Error Structure of Remote Sensing Soil Moisture Product

3.1. Obtaining the Soil Moisture Reference Dataset

The MODIS albedo and daily LST products are applied to calculate the daily ATI from May 1, 2015, to September 30, 2015 with Equation (7). The temporal ATI mean values at each pixel represent the finer spatial distribution of the SM versus the ground-based observations (Figure 3a). To spatially extend the measurement information of the ground-based sites, the relationship model between the ATI and SM is built using in-situ observations and their corresponding ATI at pixels from May 2015 to September 2015. A monotonically increasing natural logarithm function is fitted with a goodness of fit value of 0.732 (Figure 3c), which is employed to transform the ATI data into SM values at a spatial resolution of 1 km with Equation (8). To match the RS SM products in space, the transformed SM is resampled to 25 km as reference data, which represent the fact that SM values are higher on the southeast of the TP where the South Asian monsoon leads to a great deal of water vapor in the summer (Figure 3b).

Table 1 shows the validation result of applicability of ATI-based SM in the Naqu and Babao regions. The average biases of the mean values of the temporal ATI-based SM relative to those of the ground-based observations are $0.006 \text{ cm}^3/\text{cm}^3$, meaning that the ATI-based SM has fine unbiasedness on the expectation. The amplitude bias of the ATI-based SM is estimated using the TC method along with the relative truth and GLDAS data. The closer that the α value is to 1, the smaller the amplitude bias of the ATI-based SM is. Therefore, the ATI-based SM has excellent systematic unbiasedness, showing a high α value and low temporal mean bias, meaning that it is feasible to spatially expand the information of limited ground-based observations by building the relationship with the remotely sensed data for obtaining reference data. In addition, the high systematic bias of the GLDAS SM in validation regions indicates that it is risky to evaluate other RS SM products by referencing the nonvalidated modeled data.

Table 1. Validation of systematic unbiasedness of ATI-based SM.

Region \ Index	Babao			Naqu		
	Relative Truth	ATI-Based	GLDAS	Relative Truth	ATI-Based	GLDAS
Mean (cm^3/cm^3)	0.268	0.272	0.183	0.191	0.183	0.133
α in Equation (1)	1.0	0.768	0.707	1.0	0.891	0.319

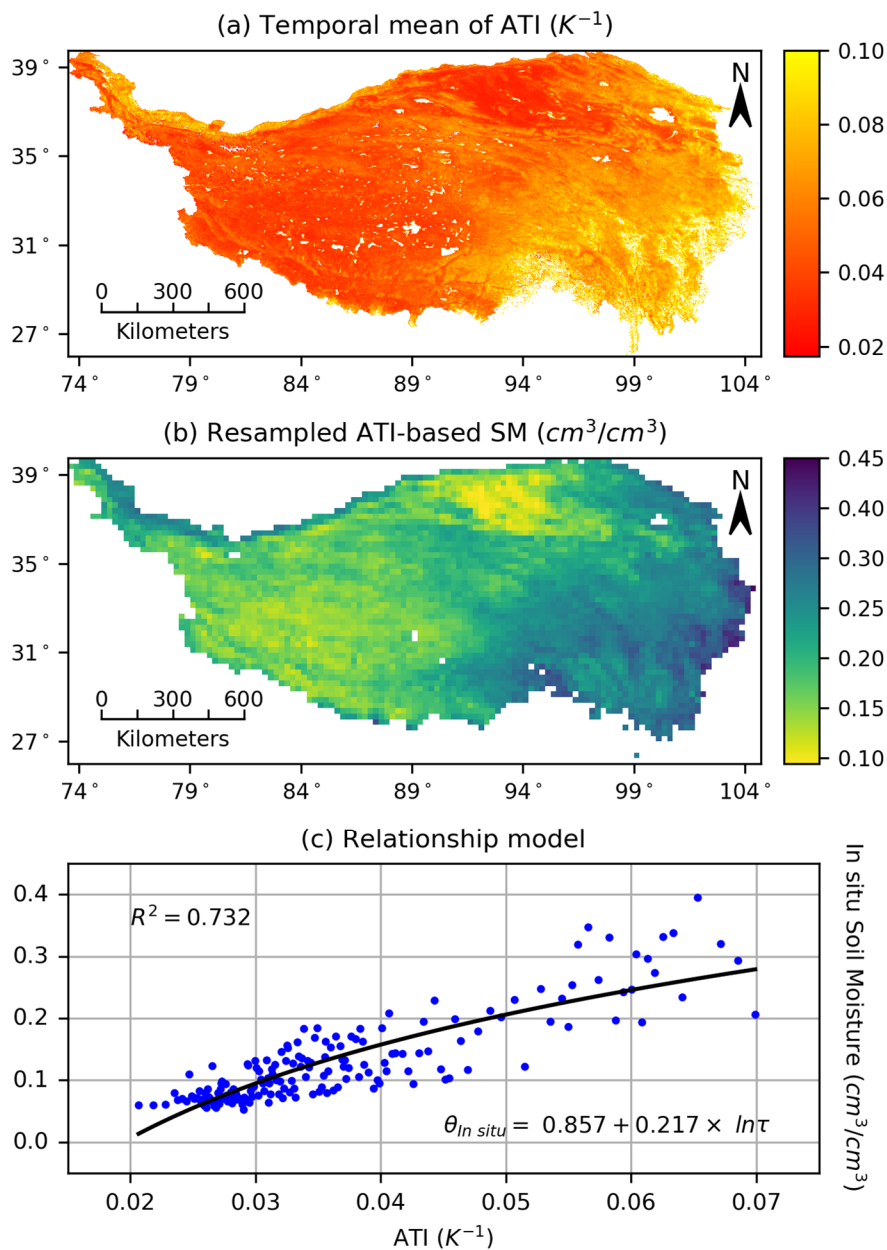


Figure 3. Spatial distribution of the averaged apparent thermal inertia (ATI) (a); the ATI-based SM is resampled to 25 km to match remote sensing (RS) SM products (b); and the relationship model between the ATI and the ground-based observations (c).

3.2. Error Decomposition

The random errors are partitioned from three collocated datasets (Figure 4), and there are larger random errors in the southeast of the TP, where the SM values are high. The averaged random errors of the ATI-based, SMAP, and AMSR2 SM are $0.034 \text{ cm}^3/\text{cm}^3$, $0.022 \text{ cm}^3/\text{cm}^3$, and $0.044 \text{ cm}^3/\text{cm}^3$, respectively. Compared with the other two datasets, the SMAP SM observed by the microwave L-band with a high sensitivity to the SM has the smallest random error.

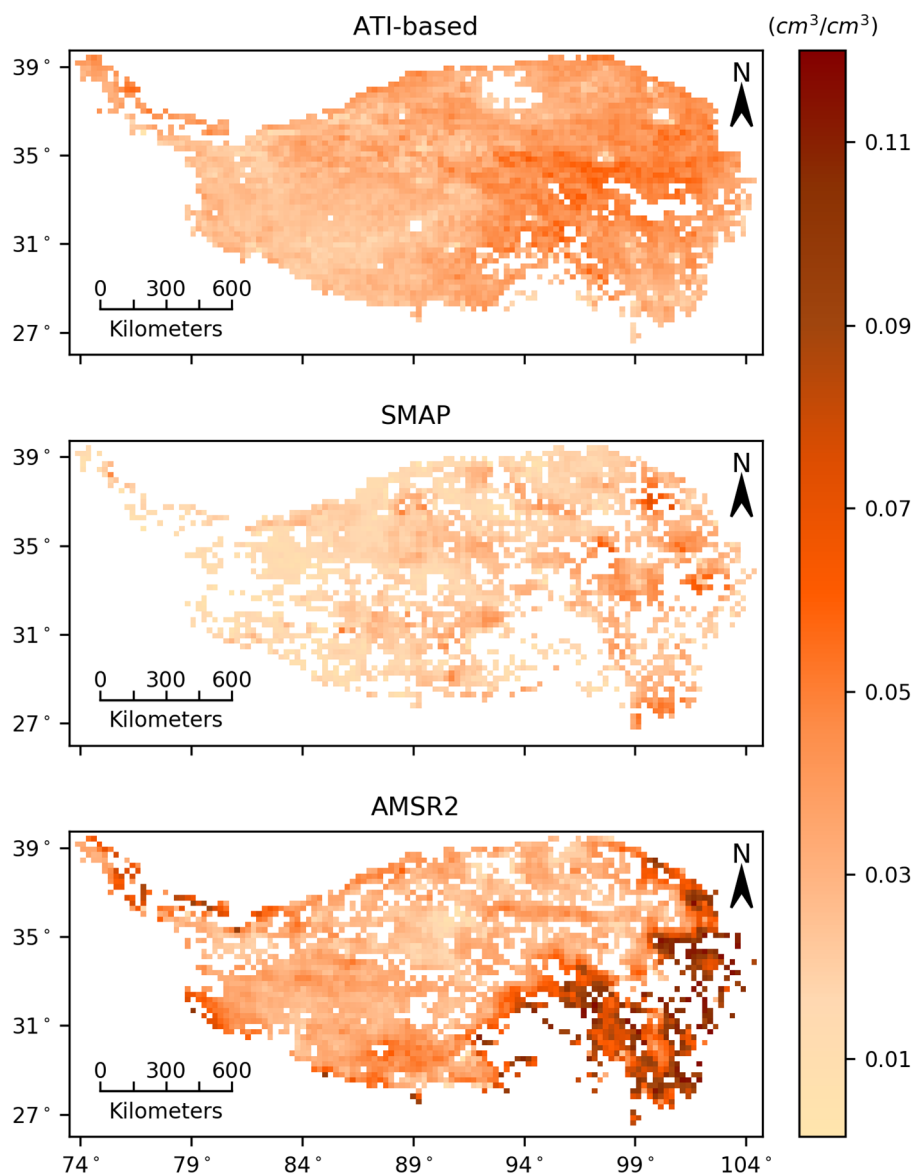


Figure 4. Spatial distributions of the random errors of RS SM products.

The systematic error generally includes the biases of the temporal mean and amplitude values. The mean values β_i can be calculated with $E(S_i)$, and since the random errors are already estimated, only the uncertainty of the amplitude is unknown in Equation (2) and can be calculated by subtracting the temporal mean bias and random errors from the total error $RMSE(S_i, S_j)$. The uncertainty of the amplitude can also be estimated with Equations (5) and (6), where the multiplicative factor of the ATI-based SM data is equal to 1.0. The systematic errors of the RS SM data are shown in Figure 5, and the averaged absolute values (Abs) of the temporal mean biases on the TP are $0.114 \text{ cm}^3/\text{cm}^3$ for the SMAP SM and $0.067 \text{ cm}^3/\text{cm}^3$ for the AMSR2 SM, accounting for 80.70% and 41.90%, respectively, of their total errors. The averaged RMSEs of the amplitudes of both SMAP and AMSR2 SM are $0.014 \text{ cm}^3/\text{cm}^3$ and $0.024 \text{ cm}^3/\text{cm}^3$, respectively. The evaluation of the amplitude avoids the influences of random errors. The amplitude uncertainty of the AMSR2 SM is higher than that of the SMAP SM on the southeastern TP, and the same is true for the random errors.

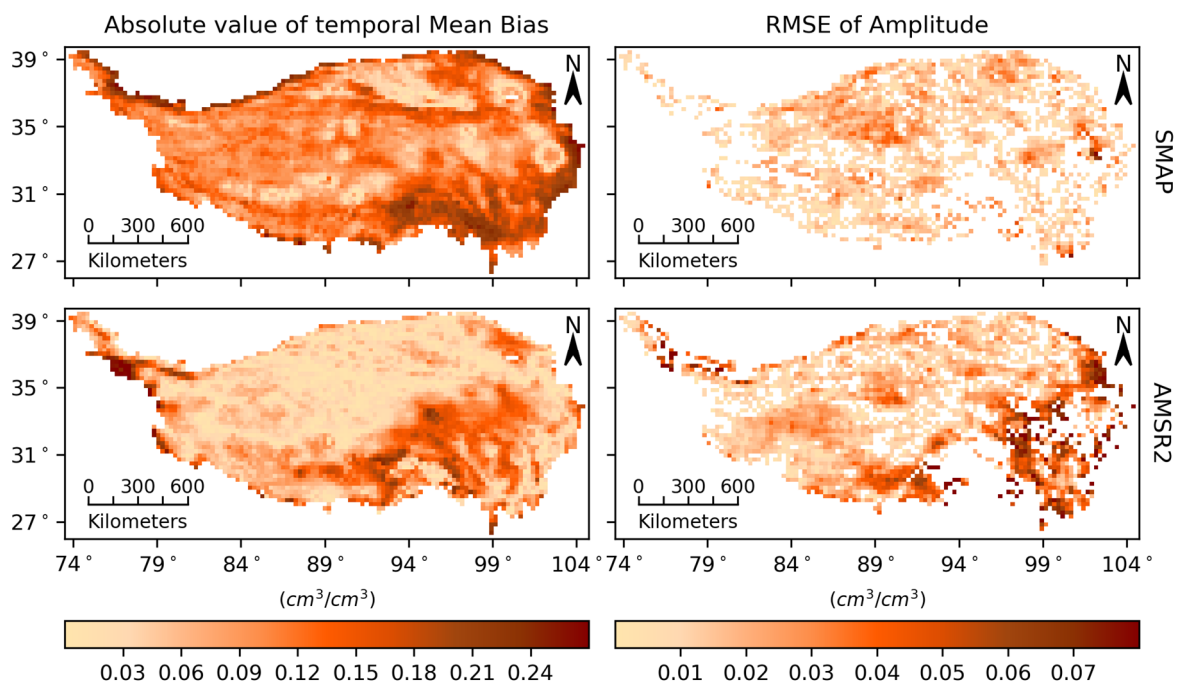


Figure 5. Systematic errors of Soil Moisture Active Passive Mission (SMAP) and Advanced Microwave Scanning Radiometer 2 (AMSR2) showing the biases of the temporal mean and amplitude values.

3.3. Analysis of Systematic Errors

Figure 6 shows the biases of both temporal mean and amplitude calculated by referencing the ATI-based SM. The temporal mean of the SMAP SM in nearly the entire region is underestimated. The temporal mean of the AMSR2 SM in 72.4% of study area is overestimated. The temporal mean of both remotely sensed SM products shows high biases deviating by approximately $0.20 \text{ cm}^3/\text{cm}^3$ on the southeastern TP, where there are high SM values according to Figure 3b, indicating the low retrieval accuracy of the SMAP and AMSR2 SM for the temporal mean in the region with high SM values.

The amplitude bias of the SMAP and AMSR2 SM can be evaluated by the multiplicative factor α_i in Equation (1). When the ATI-based SM is regarded as reference data, the α_i of the SMAP and AMSR2 SM can be calculated with Equation (6), avoiding the influences of random errors, which is different from the traditional estimation of the parameter α_i through establishing a linear model with ordinary least squares (OLS). As shown in Figure 6, the amplitude of the AMSR2 SM is obviously amplified in 83.5% of the study area. Combined with the previous analysis, this finding shows that the AMSR2 SM has large systematic and random errors in the region with high SM values. The amplitude of the SMAP SM is reduced on the northern TP but amplified on the southern TP. Unlike the AMSR2 SM, the accuracy in the amplitude of the SMAP SM is not significantly affected by high SM. The systematic errors of both remotely sensed products have spatial stratification heterogeneity, indicating that it is possible to use a small number of statistical models for the calibration of the systematic error.

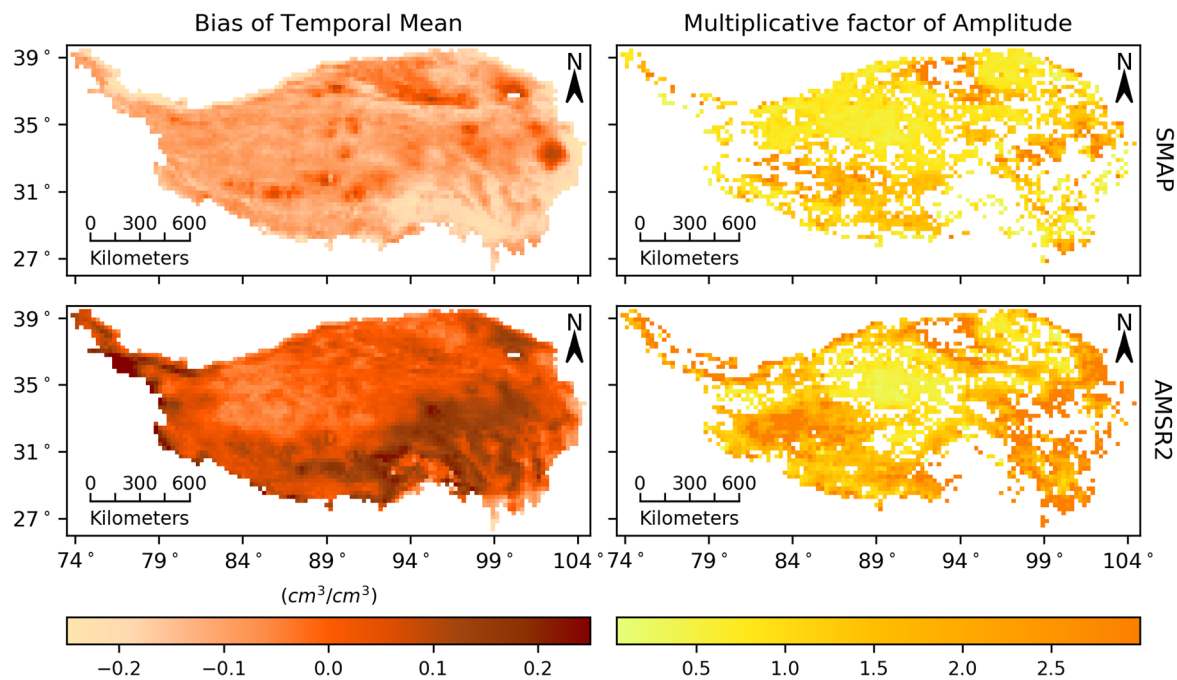


Figure 6. Absolute biases of both temporal mean and amplitude.

3.4. Ground-based Validation of Error Decomposition

The averaged ground-based observations from the Babao and Naqu regions as the relative truth, along with the ATI-based, SMAP and AMSR2 SM (Figure 7), are adopted to analyze the feasibility of the TC method regarding the error decomposition of RS SM products. The ATI-based SM as reference data is expected to be systematically unbiased, which can be validated through a comparison with the relative truth. The differences in the mean value and amplitude between the ATI-based SM and the relative truth are small (Table 2), which is caused by the high correlation between the ATI and SM, represented by a correlation coefficient of 0.856. The ATI-based SM suitably inherits the systematic component of the ground-based observation. Compared with relative truth, the amplitude biases of the ATI-based SM shown in Tables 1 and 2, introducing modeled and remotely sensed SM data into the TC method, respectively, are almost the same, demonstrating that the TC method for estimating the amplitude variance is stable. Though the samples mentioned by Zwieback et al. are not adequate [38], the error decompositions of RS SM products in Table 2 are reasonable combining with Figure 7. Therefore, it is feasible to transform RS ancillary data that are closely related to the SM as reference data to analyze the error structure of RS SM datasets with the TC method. However, if the ATI-based SM is directly employed to evaluate the total error of RS SM datasets, the random error of the ATI-based SM as a redundant item in Equation (2) should be removed to improve the accuracy of the RMSE index.

Table 2. Statistical analysis of components of the multiple-source SM data.

(cm ³ /cm ³)	Babao				Naqu			
	Relative Truth	ATI-Based	SMAP	AMSR2	Relative Truth	ATI-Based	SMAP	AMSR2
SD(ϵ_i)	0.017	0.018	0.019	0.062	0.009	0.034	0.026	0.026
SD($\alpha_i\theta$)	0.032	0.024	0.014	0.044	0.052	0.046	0.085	0.069
β_i	0.268	0.272	0.153	0.367	0.191	0.183	0.162	0.245

Note: SD(ϵ_i) and SD($\alpha_i\theta$) are standard deviations of both random errors and amplitudes, respectively.

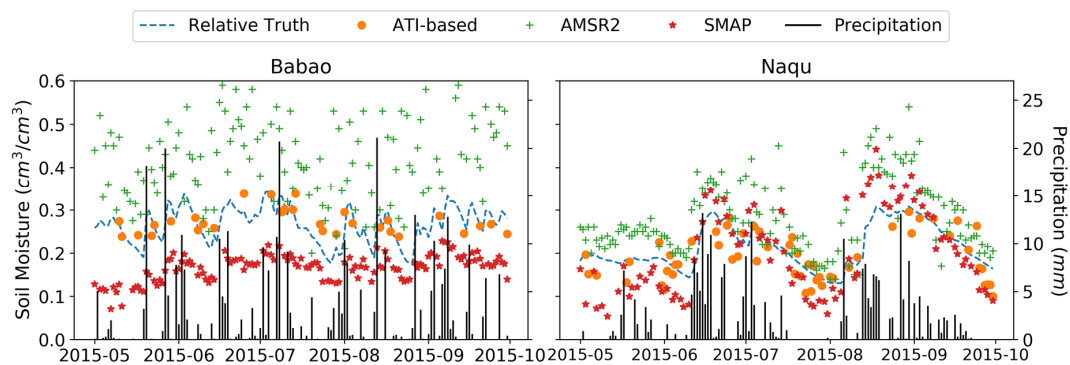


Figure 7. Differences in various SM data in the Babao and Naqu regions.

4. Conclusions

The validation of RS SM products is an important precondition of their application. The accuracy of datasets can be improved by analyzing the error structure. To decompose the errors of RS SM datasets, the temporal SM data are expressed by the sum of three components, including the temporal mean value, the amplitude, and the random error. The first two components reflect the systematic changes at the annual and seasonal scales, respectively. The objective of this study was to obtain the biases of the temporal mean and amplitude values and the variance of the random error.

To estimate the systematic biases of datasets, a reliable reference dataset is required. Ground-based measurements are commonly used as reference data in validation work; however, they are limited to a specific geographic space. The remotely sensed ATI data related to the SM are transformed into reference data to spatially extend the evaluation of RS SM datasets. To accurately assess the systematic biases of different RS SM datasets, the transformed reference data should be systematically unbiased depending on the correlation between the SM and the RS ancillary variable. It is meaningful to develop a reliable RS ancillary variable that is closely related to the SM to promote validation studies of RS SM datasets.

In this paper, the ATI-based SM as reference data combined with the TC method was applied to obtain the error structure of the SMAP and AMSR2 SM. The mean biases of the SMAP and AMSR2 SM are universal on the TP, with a large mean bias on the southeastern TP, where there is a high SM value. The amplitude bias and random error of the AMSR2 SM are more significant than those of the SMAP SM in regions with high SM values. The SMAP and AMSR2 SM cannot always retain their own advantages regarding the systematic or the random error at each pixel. Therefore, accurately determining the error structure can provide a strong basis to better understand the accuracy of RS SM datasets, which is beneficial to validation and calibration studies of RS SM datasets.

Author Contributions: J.K. designed the work, conceived of the idea, and analyzed the results. J.K. wrote this manuscript. R.J., X.L., and Y.Z. provided suggestions. All authors have read and agreed to the published version of the manuscript.

Funding: This work was supported by the Strategic Priority Research Program of the Chinese Academy of Science (Grant No. XDA19070104) and the National Natural Science Foundation of China (Grant Nos. 41531174 and 41701419).

Conflicts of Interest: The authors declare no conflict of interest.

References

1. Tuttle, S.; Salvucci, G. Empirical evidence of contrasting soil moisture–precipitation feedbacks across the united states. *Science* **2016**, *352*, 825–828. [[CrossRef](#)]
2. Stéfanon, M.; Drobinski, P.; D’Andrea, F.; Lebeau-pin-Brossier, C.; Bastin, S. Soil moisture-temperature feedbacks at meso-scale during summer heat waves over western europe. *Clim. Dyn.* **2014**, *42*, 1309–1324. [[CrossRef](#)]

3. Mystakidis, S.; Davin, E.L.; Gruber, N.; Seneviratne, S.I. Influence of soil moisture-carbon cycle interactions on the terrestrial carbon cycle over Europe. In Proceedings of the EGU General Assembly Conference, Vienna, Austria, 17–22 April 2016; 2016; p. 14125.
4. Ochsner, T.E.; Cosh, M.H.; Cuenca, R.H.; Dorigo, W.A.; Draper, C.S.; Hagimoto, Y.; Kerr, Y.H.; Njoku, E.G.; Small, E.E.; Zreda, M. State of the art in large-scale soil moisture monitoring. *Soil Sci. Soc. Am. J.* **2013**, *77*, 1888–1919. [[CrossRef](#)]
5. Seneviratne, S.I.; Corti, T.; Davin, E.L.; Hirschi, M.; Jaeger, E.B.; Lehner, I.; Orlowsky, B.; Teuling, A.J. Investigating soil moisture–climate interactions in a changing climate: A review. *Earth Sci. Rev.* **2010**, *99*, 125–161. [[CrossRef](#)]
6. Vinnikov, K.Y.; Robock, A.; Qiu, S.; Entin, J.K. Optimal design of surface networks for observation of soil moisture. *J. Geophys. Res. Atmos.* **1999**, *104*, 19743–19749. [[CrossRef](#)]
7. Liu, Y.Y.; Dorigo, W.A.; Parinussa, R.M.; de Jeu, R.A.M.; Wagner, W.; McCabe, M.F.; Evans, J.P.; van Dijk, A.I.J.M. Trend-preserving blending of passive and active microwave soil moisture retrievals. *Remote Sens. Environ.* **2012**, *123*, 280–297. [[CrossRef](#)]
8. Gruber, A.; Dorigo, W.A.; Crow, W.; Wagner, W. Triple collocation-based merging of satellite soil moisture retrievals. *IEEE Trans. Geosci. Remote Sens.* **2017**, *55*, 6780–6792. [[CrossRef](#)]
9. Ni-Meister, W. Recent advances on soil moisture data assimilation. *Phys. Geogr.* **2008**, *29*, 19–37. [[CrossRef](#)]
10. Wagner, W.; Scipal, K.; Pathe, C.; Gerten, D.; Lucht, W.; Rudolf, B. Evaluation of the agreement between the first global remotely sensed soil moisture data with model and precipitation data. *J. Geophys. Res. Atmos.* **2003**, *108*. [[CrossRef](#)]
11. Reichle, R.H.; Koster, R.D. Bias reduction in short records of satellite soil moisture. *Geophys. Res. Lett.* **2004**, *31*. [[CrossRef](#)]
12. Al-Yaari, A.; Wigneron, J.P.; Ducharne, A.; Kerr, Y.; de Rosnay, P.; de Jeu, R.; Govind, A.; Al Bitar, A.; Albergel, C.; Muñoz-Sabater, J.; et al. Global-scale evaluation of two satellite-based passive microwave soil moisture datasets (smos and amsr-e) with respect to land data assimilation system estimates. *Remote Sens. Environ.* **2014**, *149*, 181–195. [[CrossRef](#)]
13. Al-Yaari, A.; Wigneron, J.-P.; Ducharne, A.; Kerr, Y.; Wagner, W.; De Lannoy, G.; Reichle, R.; Al Bitar, A.; Dorigo, W.; Richaume, P. Global-scale comparison of passive (smos) and active (ascats) satellite based microwave soil moisture retrievals with soil moisture simulations (merra-land). *Remote Sens. Environ.* **2014**, *152*, 614–626. [[CrossRef](#)]
14. Fang, L.; Hain, C.R.; Zhan, X.; Anderson, M.C. An inter-comparison of soil moisture data products from satellite remote sensing and a land surface model. *Int. J. Appl. Earth Obs. Geoinf.* **2016**, *48*, 37–50. [[CrossRef](#)]
15. Brocca, L.; Hasenauer, S.; Lacava, T.; Melone, F.; Moramarco, T.; Wagner, W.; Dorigo, W.; Matgen, P.; Martínez-Fernández, J.; Llorens, P. Soil moisture estimation through ascats and amsr-e sensors: An intercomparison and validation study across europe. *Remote Sens. Environ.* **2011**, *115*, 3390–3408. [[CrossRef](#)]
16. Burgin, M.S.; Colliander, A.; Njoku, E.G.; Chan, S.K.; Cabot, F.; Kerr, Y.H.; Bindlish, R.; Jackson, T.J.; Entekhabi, D.; Yueh, S.H. A comparative study of the smap passive soil moisture product with existing satellite-based soil moisture products. *IEEE Trans. Geosci. Remote Sens.* **2017**, *55*, 2959–2971. [[CrossRef](#)] [[PubMed](#)]
17. Gruhier, C.; Rosnay, P.d.; Hasenauer, S.; Holmes, T.; Jeu, R.d.; Kerr, Y.; Mougou, E.; Njoku, E.; Timouk, F.; Wagner, W. Soil moisture active and passive microwave products: Intercomparison and evaluation over a sahelian site. *Hydrol. Earth Syst. Sci.* **2010**, *14*, 141–156. [[CrossRef](#)]
18. Ma, C.; Li, X.; Chen, K. The discrepancy between backscattering model simulations and radar observations caused by scaling issues: An uncertainty analysis. *IEEE Trans. Geosci. Remote Sens.* **2019**, *57*, 5356–5372. [[CrossRef](#)]
19. Nykanen, D.K.; Foufoula-Georgiou, E. Soil moisture variability and scale-dependency of nonlinear parameterizations in coupled land–atmosphere models. *Adv. Water Res.* **2001**, *24*, 1143–1157. [[CrossRef](#)]
20. Guevara, M.; Vargas, R. Downscaling satellite soil moisture using geomorphometry and machine learning. *PLoS ONE* **2019**, *14*, e0219639. [[CrossRef](#)]
21. Kang, J.; Jin, R.; Li, X. Regression kriging-based upscaling of soil moisture measurements from a wireless sensor network and multiresource remote sensing information over heterogeneous cropland. *IEEE Geosci. Remote Sens. Lett.* **2015**, *12*, 92–96. [[CrossRef](#)]

22. Kang, J.; Jin, R.; Li, X.; Ma, C.; Qin, J.; Zhang, Y. High spatio-temporal resolution mapping of soil moisture by integrating wireless sensor network observations and modis apparent thermal inertia in the babao river basin, china. *Remote Sens. Environ.* **2017**, *191*, 232–245. [[CrossRef](#)]
23. Merlin, O.; Malbêteau, Y.; Noffi, Y.; Bacon, S.; Khabba, S.E.-R.S.; Jarlan, L. Performance metrics for soil moisture downscaling methods: Application to dispatch data in central morocco. *Remote Sens.* **2015**, *7*, 3783–3807. [[CrossRef](#)]
24. Peng, J.; Loew, A.; Zhang, S.; Wang, J.; Niesel, J. Spatial downscaling of satellite soil moisture data using a vegetation temperature condition index. *Geosci. Remote Sens. IEEE Trans.* **2016**, *54*, 558–566. [[CrossRef](#)]
25. Piles, M.; Camps, A.; Vall-Llossera, M.; Corbella, I.; Panciera, R.; Rüdiger, C.; Kerr, Y.H.; Walker, J. Downscaling smos-derived soil moisture using modis visible/infrared data. *Geosci. Remote Sens. IEEE Trans.* **2011**, *49*, 3156–3166. [[CrossRef](#)]
26. Drusch, M.; Wood, E.F.; Gao, H. Observation operators for the direct assimilation of trmm microwave imager retrieved soil moisture. *Geophys. Res. Lett.* **2005**, *32*. [[CrossRef](#)]
27. Cosh, M.H.; Jackson, T.J.; Starks, P.; Heathman, G. Temporal stability of surface soil moisture in the little washita river watershed and its applications in satellite soil moisture product validation. *J. Hydrol.* **2006**, *323*, 168–177. [[CrossRef](#)]
28. Gruber, A.; Su, C.H.; Zwieback, S.; Crow, W.; Dorigo, W.; Wagner, W. Recent advances in (soil moisture) triple collocation analysis. *Int. J. Appl. Earth Obs. Geoinf.* **2016**, *45*, 200–211. [[CrossRef](#)]
29. Miyaoka, K.; Gruber, A.; Ticconi, F.; Hahn, S.; Wagner, W.; Figa-Saldaña, J.; Anderson, C. Triple collocation analysis of soil moisture from metop-a ascats and smos against jra-55 and era-interim. *IEEE J. Sel. Top. Appl. Earth Obs. Remote Sens.* **2017**, *10*, 2274–2284. [[CrossRef](#)]
30. Dorigo, W.; Scipal, K.; Parinussa, R.; Liu, Y.; Wagner, W.; De Jeu, R.; Naeimi, V. Error characterisation of global active and passive microwave soil moisture datasets. *Hydrol. Earth Syst. Sci.* **2010**, *14*, 2605–2616. [[CrossRef](#)]
31. Su, Z.; Wen, J.; Dente, L.; Velde, R.; Wang, L.; Ma, Y.; Yang, K.; Hu, Z. The tibetan plateau observatory of plateau scale soil moisture and soil temperature (tibet-obs) for quantifying uncertainties in coarse resolution satellite and model products. *Hydrol. Earth Syst. Sci.* **2011**, *15*, 2303–2316. [[CrossRef](#)]
32. Rodell, M.; Houser, P.R.; Jambor, U.; Gottschalck, J.; Mitchell, K.; Meng, C.J.; Arsenault, K.; Cosgrove, B.; Radakovich, J.; Bosilovich, M.; et al. The global land data assimilation system. *Bull. Am. Meteorol. Soc.* **2004**, *85*, 381–394. [[CrossRef](#)]
33. Vrije Universiteit Amsterdam (Richard de Jeu); NASA GSFC (Manfred Owe). *AMSR2/GCOM-W1 Surface Soil Moisture (LPRM) L3 1 Day 25 km x 25 km Ascending/Descending V001*; Goddard Earth Sciences Data, Information Services Center (GES DISC) (Bill Teng), Eds.; Goddard Earth Sciences Data and Information Services Center (GES DISC): Greenbelt, MD, USA, 2014. [[CrossRef](#)]
34. O'Neill, P.E.; Chan, S.; Njoku, E.G.; Jackson, T.; Bindlish, R.; Chaubell, J. *SMAP L3 Radiometer Global Daily 36 km EASE-Grid Soil Moisture, Version 6*; NASA National Snow and Ice Data Center Distributed Active Archive Center: Boulder, CO, USA, 2019. [[CrossRef](#)]
35. Gruber, A.; De Lannoy, G.; Albergel, C.; Al-Yaari, A.; Brocca, L.; Calvet, J.C.; Colliander, A.; Cosh, M.; Crow, W.; Dorigo, W.; et al. Validation practices for satellite soil moisture retrievals: What are (the) errors? *Remote Sens. Environ.* **2020**, *244*, 111806. [[CrossRef](#)]
36. McColl, K.A.; Vogelzang, J.; Konings, A.G.; Entekhabi, D.; Piles, M.; Stoffelen, A. Extended triple collocation: Estimating errors and correlation coefficients with respect to an unknown target. *Geophys. Res. Lett.* **2014**, *41*, 6229–6236. [[CrossRef](#)]
37. Van doninck, J.; Peters, J.; De Baets, B.; De Clercq, E.M.; Ducheyne, E.; Verhoest, N.E.C. The potential of multitemporal aqua and terra modis apparent thermal inertia as a soil moisture indicator. *Int. J. Appl. Earth Obs. Geoinf.* **2011**, *13*, 934–941. [[CrossRef](#)]
38. Zwieback, S.; Scipal, K.; Dorigo, W.; Wagner, W. Structural and statistical properties of the collocation technique for error characterization. *Nonlinear Process. Geophys.* **2012**, *19*, 69–80. [[CrossRef](#)]

